

THESIS FOR THE DEGREE OF LICENTIATE OF ENGINEERING

**Probing the effect of UV radiation on the
chemistry in circumstellar envelopes around
evolved stars**

MARYAM SABERI



CHALMERS

Department of Earth and Space Sciences
CHALMERS UNIVERSITY OF TECHNOLOGY
Gothenburg, Sweden 2016

Probing the effect of UV radiation on the chemistry in circumstellar envelopes around evolved stars

MARYAM SABERI

© Maryam Saberi, 2016

Radio Astronomy & Astrophysics Group
Department of Earth and Space Sciences
Chalmers University of Technology
SE-412 96 Gothenburg, Sweden
Phone: +46 (0)31-772 1000

Contact information:

Maryam Saberi
Onsala Space Observatory
Chalmers University of Technology
SE-439 92 Onsala, Sweden

Phone: +46 (0)31-772 5546

Fax: +46 (0)31-772 5590

Email: maryam.saberi@chalmers.se

Printed by Chalmers Reproservice
Chalmers University of Technology
Gothenburg, Sweden 2016

Probing the effect of UV radiation on the chemistry in circumstellar envelopes around evolved stars

MARYAM SABERI

Department of Earth and Space Sciences
Chalmers University of Technology

Abstract

Low to intermediate mass ($0.8 - 8 M_{\odot}$) stars lose a substantial amount of their mass in the last phase of stellar evolution, the asymptotic giant branch (AGB) phase. Hence, they are one of the main suppliers of dust and gas in the interstellar medium and important for the enrichment of galaxies. Due to the intense mass loss, a circumstellar envelope (CSE), rich in gas and dust, forms around AGB stars. The exact mechanism(s) responsible for the mass loss is not yet fully established, although a radiatively driven dust wind appears to play a major role.

CSEs are excellent laboratories to understand the mass loss process as well as to constrain stellar properties. It is known that ultra-violet (UV) photons play a critical role in the chemical composition and evolution of the CSEs. The UV photons that can impact the chemistry of the CSE originate, in the inner part, from stellar chromospheric activity or hot binary companions. In the outer part they come from the interstellar radiation field (ISRF). However, the ISRF is the only UV source which has been considered to affect the photo-chemistry of the CSEs. It was long expected that the stellar UV emission is weak and that its effects would not be noticeable, especially not using single-dish telescope observations. Now, high-spatial resolution interferometric observations and increasing number of detections of stellar UV sources indicate the importance of considering the internal UV radiation in the CSEs chemistry.

In order to study this effect, we have started an analysis of the carbon-type AGB star, R Scl. Previous studies show a variation of the $^{12}\text{CO}/^{13}\text{CO}$ ratio in the circumstellar envelope and a discrepancy between the circumstellar $^{12}\text{CO}/^{13}\text{CO}$ ratio and the photospheric $^{12}\text{C}/^{13}\text{C}$ ratio, which has been explained as a result of internal UV radiation. Our detailed radiative transfer modelling of H^{12}CN and H^{13}CN isotopologues around R Scl confirms this proposed scenario. This result highlights the importance of considering all the potential UV sources on the chemistry of the CSE of R Scl.

Applying our suggested method of quantifying the effect of the internal UV radiation field to a large number of AGB stars might help to investigate the binarity rate of AGBs. This will also improve our understanding of the stellar chromospheric activity. These are both open questions in the field of research on AGB stars.

Keywords: Stars: abundances - Stars: AGB - Stars: individual: R Scl - Stars: binaries - Stars: carbon - Stars: circumstellar matter - Stars: chromospheres - Ultraviolet: stars

Research contributions

This thesis is based on the work contained in the following paper:

- M. Saberi, M. Maercker, E. De. Beck, W. H. T. Wlemmings, H. Olofsson, T. Danilovich:
H¹²CN and H¹³CN excitation analysis in the circumstellar outflow of R Scl
Accepted to publish in *Astronomy & Astrophysics*, (2016)

Other Publications

I also participated in the following paper not included in the thesis:

- A. Javadi, M. Saberi, J. T. van Loon, H. Khosroshahi, N. Golabatooni, M. T. Mir-torabi :
The UK Infrared Telescope M33 monitoring project - IV. Variable red giant stars across the galactic disc
Monthly Notices of the Royal Astronomical Society, .447.3973J (2015)

Acknowledgements

I would like to express my special thanks to my supervisor, Prof. Wouter Vlemmings, for his continued support, encouragement and patience. Thanks for all stimulating scientific discussions and valuable feedbacks. I really appreciate your prompt responses to my emails and questions.

Many thanks to my co-supervisors Dr. Matthias Maercker and Dr. Elvire De Beck for all valuable feedbacks, discussions and patience in reading and correcting my texts. Thanks for sharing your own experiences with me. Special thanks to my examiner, Prof. Hans Olofsson, for brilliant comments, suggestions and expert advice. Many thanks to Prof. John Black for all valuable and inspiring discussions. I would also like to thank Dr. Theo Khouri for reading my thesis and the insightful comments.

Many thanks to my fellow PhD students, Postdocs and colleagues at Onsala Space Observatory and Department of Earth and Space Sciences at Chalmers University of technology, for making a friendly and inspiring working environment. To my office mate and a very good friend, Daria. Thanks for all good moments and laughs with had together.

Thanks to all my Iranian friends in Gothenburg who made me feel home and for making these past few years of greatest. Thanks to Mitra, Parisa, Fatemeh and Elnaz for your inestimable friendship.

I would also thank to my masters supervisors Dr. Atefeh Javadi and Dr. Jacco van Loon who encouraged me to pursue Astronomy.

Special thanks go to my lovely family who always support all my decisions. Thanks for your unwavering love, unconditional support and encouragement throughout all my studies. This thesis is dedicated to you.

Maryam

Contents

Abstract	i
Research contributions	iii
Other publications	iii
Acknowledgements	v
1 Introduction	1
1.1 Astrochemistry	1
1.2 Stellar Evolution	1
1.3 AGB characteristics	3
1.3.1 AGB structure	4
1.3.2 Mass Loss	5
1.4 Chemical evolution	6
1.4.1 CSE chemistry	6
1.4.2 Isotopologue ratio	7
2 Radiative Transfer Modelling	11
2.1 Molecular transitions	11
2.2 Radiative rates	12
2.3 Radiative Transfer Modelling	13
2.4 Accelerated Lambda Iteration method	16
3 The effect of UV radiation on the chemistry in CSEs	17
3.1 Potential UV-radiation fields	17
3.1.1 External UV radiation - ISRF	17
3.1.2 Internal UV radiation - Chromospheric activity	18
3.1.3 Internal UV radiation - Binary companions	19
3.2 Molecular photodissociation by UV radiation	19
4 Chemical Modelling	23
4.1 The CSE code	23
4.1.1 The chemical network	24

4.1.2 Photodissociation of CO	25
5 Introduction to Paper I	27
References	29

Chapter 1

Introduction

General references: Habing & Olofsson (2003) ; LeBlanc (2010)

1.1 Astrochemistry

The aim of astrochemistry is understanding the physical and chemical conditions in astrophysical environments. Observations and modelling of chemical species can be used to probe the physical properties of astrophysical regions.

Stars are excellent laboratories for studying the physics in extreme conditions which are unreachable or very expensive to do on earth. As seen in Fig. 1.1, almost all heavy elements in the periodic table, including the essential ones for life (e.g. C, N and O) are produced inside the stars through nucleosynthesis. The heavy elements which are produced in the stellar interior are blown out into space during the last phases of stellar evolution. In this thesis, we aim to make a more complete chemical picture of the molecular-rich environment around evolved stars.

1.2 Stellar Evolution

Stars are gravitationally-bound spheres of plasma. They are born in giant and cold molecular hydrogen clouds. Gravity triggers formation of a protostar by contraction of interstellar clouds. The contraction leads to increasing central density and temperature of the protostar. Once the temperature of the protostar becomes high enough for hydrogen nuclear burning ($T > 4 \times 10^6$ K through PP-chain and $T > 15 \times 10^6$ K through CNO cycle) in the centre, the protostar begins its life as a main-sequence (MS) star. The MS phase is the longest and most stable phase of the stellar evolution. The stellar life time and post-MS evolutionary phases de-

H												He					
Li	Be											B	C	N	O	F	Ne
Na	Mg											Al	Si	P	S	Cl	Ar
K	Ca	Sc	Ti	V	Cr	Mn	Fe	Co	Ni	Cu	Zn	Ga	Ge	As	Se	Br	Kr
Rb	Sr	Y	Zr	Nb	Mo	Tc	Ru	Rh	Pd	Ag	Cd	In	Sn	Sb	Te	I	Xe
Cs	Ba	Hf	Ta	W	Re	Os	Ir	Pt	Au	Hg	Tl	Pb	Bi	Po	At	Rn	
Fr	Ra																
		La	Ce	Pr	Nd	Pm	Sm	Eu	Gd	Tb	Dy	Ho	Er	Tm	Yb	Lu	
		Ac	Th	Pa	U	Np	Pu	Am	Cm	Bk	Cf	Es	Fm	Md	No	Lr	

Figure 1.1: The periodic table. The colors indicate some of the different nucleosynthetic sources for each element. (Credit: NAU Meteorite Laboratory).

pend on the initial mass of the star. Generally, massive stars evolve quicker than less massive stars. The MS phase lasts for approximately 10^{10} yr for a $1M_{\odot}$ star and 3×10^7 yr for a $8M_{\odot}$ star. Here, we focus on the evolutionary tracks for low-to intermediate-mass ($0.8 - 8 M_{\odot}$) stars.

To illustrate the stellar evolutionary phases, it is useful to plot a Hertzsprung-Russel (H-R) diagram which shows the relation between temperatures and luminosities of stars. These two observable quantities vary significantly during the evolution of a given star. Competition between forces of gravity and pressure due to nuclear fusion reactions plays a critical role in the stellar evolution, and determines the positions of stars in the H-R diagram. Fig. 1.2 shows the position in the H-R diagram of different mass stars on the MS phase as well as the post-MS phases of evolution for a $1M_{\odot}$ mass star. The steep path which connects the top left (high luminosity and high temperature) of the diagram to the bottom right (low luminosity and low temperature) shows the position of MS stars with different initial masses. Stars in the MS phase are in thermal and hydrostatic equilibrium, meaning that the inward force of gravity is balanced by the outward force of thermal pressure. Eventually all the hydrogen supply in the core is consumed, and the temperature is not sufficient to ignite the He burning. So, the gravity overcomes the thermal pressure and the core starts contracting. However, while the nuclear burning stops in the core, hydrogen is still burning in a shell around the inert central region. The He core becomes electron degenerate and is continuously fed by the He from the upper shell. The outer envelope becomes convective. The energy produced in the shell-burning causes the expansion of the outer layers. During this expansion, the surface temperature of the star decreases so that the star becomes colder and redder. The star evolves rapidly towards the sub-giant and then the red-giant branch (RGB) phases. The RGB phase lasts for approximately 10^9 yr for a $1M_{\odot}$ star. At the RGB, the convective envelope reaches down the inner layers

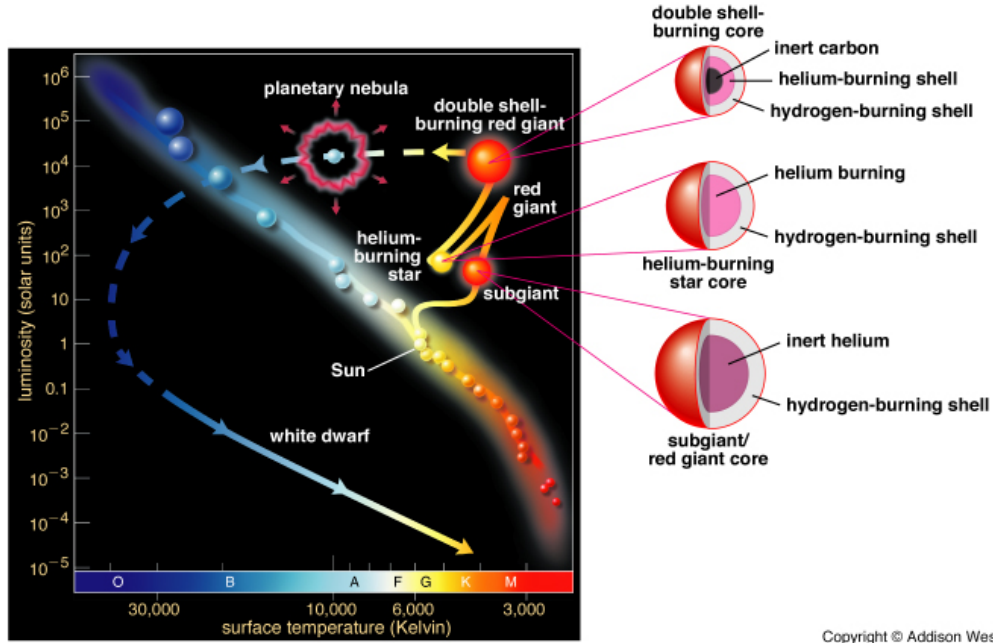
and brings the material enriched in ${}^4\text{He}$, ${}^{14}\text{N}$ and ${}^{13}\text{C}$ to the surface. This process is called the first dredge-up (FDU). The FDU happens for all stars in the RGB phase regardless of their initial masses. For stars with masses below $\sim 2 M_{\odot}$, the electrons in the core become degenerate and the gas in the core does not obey the ideal gas law, meaning that the temperature can increase without increasing the pressure. Consequently the core will rapidly get hot enough (10^8 K) for the fusion of He into carbon through the triple-alpha process. The released energy due to the fusion increases the reaction rate, causing an explosive reaction in the core, called He-core flash. The He-core flash is very short lived. The sudden increase in temperature lifts the degeneracy and the star moves downward to the Horizontal Branch (HB). The hydrostatic equilibrium will be restored again. Stars with masses higher than $2 M_{\odot}$ ignite helium under non-degenerate conditions.

During the HB phase, stars burn He in its core and hydrogen in a shell outside the core. A $1M_{\odot}$ star stays at the horizontal branch for about 10^8 yr. Eventually all the helium in the core is consumed and the star ascends to the giant branch a second time, this is called asymptotic giant branch (AGB) phase. In the AGB phase, the star has a degenerate C-O core with two distinct layers of He- and H-burning shells around the core. This is the last phase of nuclear burning for low- and intermediate-mass stars, since the temperature does not get high enough in these stars for carbon-burning to occur. The star will stay at the AGB phase around 2×10^7 yr. In the early AGB, stars with $M > 4M_{\odot}$ experience the second dredge-up (SDU). As seen in Fig. 1.2, in the AGB phase, the star has extreme values of surface temperature (very cold) and luminosity (very high). AGB stars shed a large fraction of their material into the interstellar medium (ISM) through stellar pulsations and radiation pressure. Because of instabilities in the He burning shell, AGB stars go through processes called thermal pulses. The thermally-pulsing AGB (TP-AGB) phase during the AGB typically lasts about 10^6 yr, although the exact time scale depends on the stellar mass. A more detailed description of AGB stars and their chemical evolution are presented in the following sections.

Finally, the star ends its life as a planetary nebula (PN). In the PN phase, the core shrinks to its most compact state, while the outer layers are expelled away. Eventually, the outer layers around the core are dispersed. The remaining small hot dense carbon-oxygen core with mass of roughly $0.6M_{\odot}$ is called a white dwarf. The planetary nebula phase lasts approximately 5×10^4 yr for a $1M_{\odot}$ star. Since there is no more nuclear fuel left, the white dwarf gets cooler and less luminous, and turns, theoretically, to a black dwarf.

1.3 AGB characteristics

AGB stars are giant ($R \sim 300R_{\odot}$) stars with luminosity ranging from 3000 - 20000 L_{\odot} and surface temperature of 1800 - 3000 K. Pulsations of the atmospheric layers yield variability with a period of hundreds of days. AGBs can be divided into



Copyright © Addison Wesley

Figure 1.2: The HR diagram shows the evolutionary phases for a $1M_{\odot}$ star and the MS stars with different masses. The stellar structure in the different phases of evolution for a $1M_{\odot}$ star are shown on the right hand side.

three variability types regarding the amplitude and regularity of the pulsation: Mira high-amplitude regular variable (variability > 2.5 mag in the visual), low-amplitude semi-regular variable (variability ~ 1 mag in visual) and low-amplitude irregular variables.

1.3.1 AGB structure

A schematic view of an AGB star is shown in Fig. 1.3. The star contains a dense and very hot electron-degenerate core made of carbon and oxygen, two layers of He- and H-burning, and a convective envelope.

The core of an AGB star is supported by the pressure of degenerate electrons, which implies an upper limit of $8M_{\odot}$ for the AGB. The core is cooled by neutrino emission, thus the temperature does not get high enough for the carbon burning. The stellar luminosity is provided by the double shell burning in a cyclical process. The He-burning shell becomes thermally unstable which leads to very long-term ($\sim 10^5$ yr for a $1M_{\odot}$ star) stellar variability.

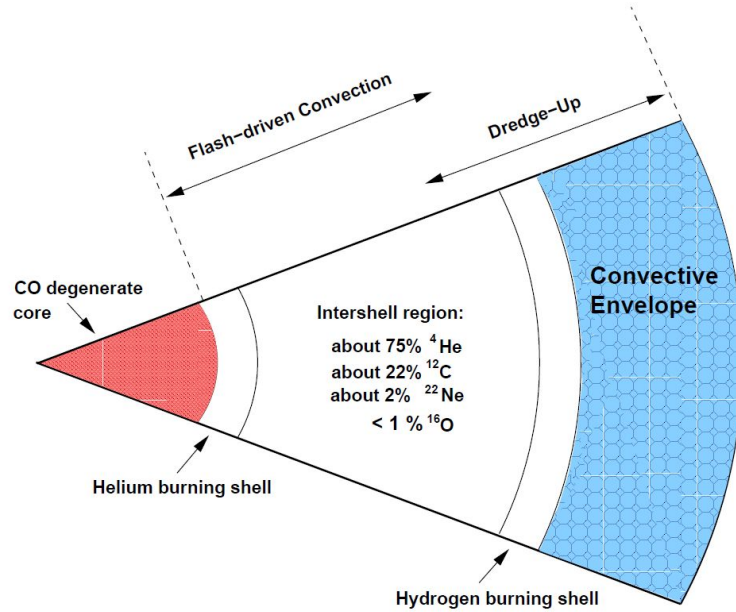


Figure 1.3: A schematic view of the structure of an AGB star (not to scale), from Karakas, Lattanzio, Pols (2002).

1.3.2 Mass Loss

In the AGB stage, the star loses up to 80 percent of its initial mass typically at rates of $10^{-8} - 10^{-4} M_{\odot} \text{ yr}^{-1}$, through the combined action of pulsations and radiation pressure. Thus, AGBs are main suppliers of molecules and dust to the interstellar medium. The mass loss rate characterizes and terminates the evolution on the AGB.

The mass-loss process initiates very close to the central star ($R < 10R_{\odot}$). In this region, radiation pressure acts on dust grains that form from gas elevated to high altitudes by stellar pulsations. Although this paradigm is widely accepted, the detailed mass-loss mechanism is not yet well understood. While dust grains are crucial for driving the wind, they comprise only at most 1 % of the mass of the outflow. Most of the remaining mass is in the form of molecular gas. At different distances from the star, different processes are important for controlling the chemistry happening in the gas. Based on these differences, we can divide the envelope into three parts: the inner, the intermediate, and the outer CSE. Figure.1.4 shows a schematic view of the CSE with the size, temperature and different chemical processes happening in different parts.

A process named thermal pulse (TP) occurs with a periodicity of $10^4 - 10^5$ yr due to the explosive He-burning in the double shell burning phase. This causes a short phase of intense mass loss that can lead to the formation of a detached shell around the given AGB star. Nowadays, high-spatial-resolution interferometric observa-

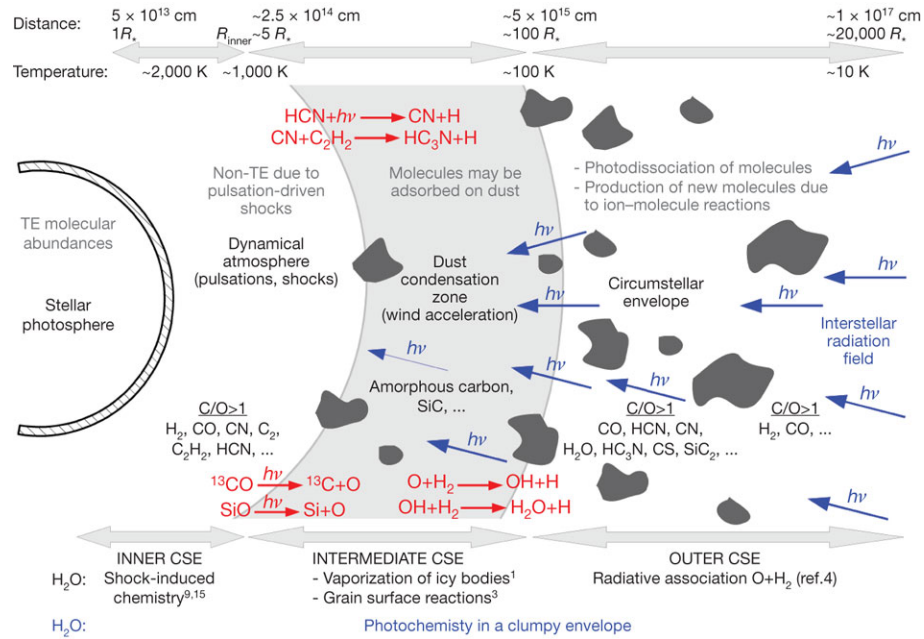


Figure 1.4: A schematic view of the CSE of an AGB star from <https://fys.kuleuven.be>.

tions, such as those obtained with the Atacama Large Millimeter/submillimeter Array (ALMA), enable us to distinguish between CSEs and detached-shells of AGB stars. Figure.1.5 shows the separation of the CSE and the detached shell of the AGB star, R Scl, in the $CO(J = 3 - 2)$ map from ALMA observations, Maercker et al. 2012. The spiral pattern observed in the CSE is due to a binary companion in a distance of approximately 60 AU from the central star.

1.4 Chemical evolution

1.4.1 CSE chemistry

There are different processes responsible for the formation of molecules around AGB stars. Photospheric species or parent species form under thermal equilibrium (TE) conditions in the photosphere where the temperature and density are high. Some parent species formed in the photosphere are injected to the CSE. The TE conditions do not hold for the layers above the photosphere due to the passage of stellar pulsations and shocks (e.g. Cherchneff 2006). Thus, many molecules are formed locally in the CSE through different chemical and radiative processes induced by cosmic rays and the interstellar radiation field. Thus, the CSE species are a combination of photospheric origin and CSE chemistry products. Molecular photodissociation by the interstellar UV radiation is the main factor in determining the molecular extension in the outer CSE. CSEs are mainly dominated by H_2

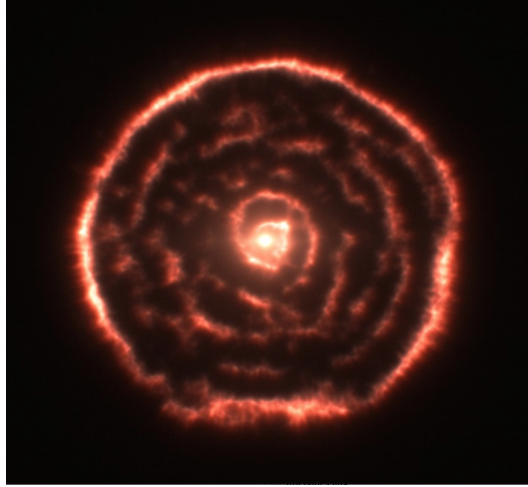


Figure 1.5: ^{12}CO ($J=3-2$) map at stellar velocity by ALMA, Maercker et al. 2012.

molecules. Table. 1.1 shows the list of molecules detected in the CSE of AGBs to date.

Generally the molecular setup and grain types of CSEs are determined by the elemental C/O ratio. AGB stars can be classified into three categories: carbon rich C-type AGBs ($\text{C/O} > 1$), S-type AGBs ($\text{C/O} \sim 1$), and oxygen rich M-type AGBs ($\text{C/O} < 1$). The envelope of C-type stars are rich in CO and other C-bearing molecules e.g. C_2 , C_2H_2 and HCN and the envelope of M-type stars are rich in CO and other O-bearing molecules such as H_2O and TiO, (e.g. Le Bertre 1997).

CO is the most abundant molecule after H_2 in the CSEs. Thus, observations of CO are widely used to determine the physical parameters of the CSE, such as the mass-loss rate, density structure, expansion-velocity profile, kinetic temperature and spatial extent (e.g. Neri et al. 1998; Schöier & Olofsson 2000; Ramstedt et al. 2008; Castro-Carrizo et al. 2010; De Beck et al. 2010). Observations of other abundant molecules are required to constrain the physical properties more precisely as well as to study the chemical network active in the CSE (e.g. Omont et al. 1993; Bujarrabal et al. 1994; Maercker et al. 2008, 2009; De Beck et al. 2012).

Known processes that may affect the chemical composition of the CSE of a solitary AGB star are shocks due to stellar pulsations, and chromospheric activity in the inner wind, gas-dust interaction in the intermediate wind, and photodissociation by the interstellar UV-radiation, associated photo-induced chemistry, and chemical fractionation processes in the outer wind.

1.4.2 Isotopologue ratio

The study of isotopic ratios of evolved stars provides important information on the stellar evolutionary phases, the initial stellar mass and the chemical enrichment

Table 1.1: Molecules detected in AGB CSEs

2 atoms:	OH	HF	C ₂	CN	CO	HCl
	SiC	SiN	AlO*	CP	CS	SiO
	PN	AlF	PO	SO	NaCl	SiS
	AlCl	KCl				
3 atoms:	H ₂ O	C ₂ H	HCN	HNC	H ₂ S	C ₃
	CCN	CO ₂	HCP	NaCN	MgCN	MgNC
	SiC ₂	AlNC	SiCN	SiNC	C ₂ P	C ₂ S
	SO ₂	KCN	SiCSi	FeCN		
4 atoms:	NH ₃	C ₂ H ₂	H ₂ CO	PH ₃	l-H ₂ C ₃	c-C ₃ H
	HC ₂ N	H ₂ CS	C ₃ N	MgC ₂ H*	HMgNC	C ₃ O
	SiC ₃	C ₃ S	NC ₂ P*			
5 atoms:	CH ₄	CH ₂ NH	SiH ₄	c-C ₃ H ₂	l-C ₃ H ₂	CH ₂ CN
	C ₄ H	HC ₃ N	HC ₂ NC	HNC ₃	C ₅	SiC ₄
6 atoms:	C ₂ H ₄	CH ₃ CN	l-H ₂ C ₄	SiH ₃ CN*	C ₅ H	HC ₄ N
	C ₅ N	C ₅ S				
≥ 7 atoms :	CH ₃ CCH	CH ₂ CHCN	C ₆ H	H ₂ C ₆	HC ₅ N	C ₇ H
	C ₈ H	HC ₇ N	HC ₉ N			
Ions:	CN ⁻	HCO ⁺	C ₃ N ⁻	C ₄ H ⁻	C ₅ N ⁻	C ₆ H ⁻
	C ₈ H ⁻					

Note: * indicates a tentative detection.

of the interstellar medium. For instance, the photospheric ¹²C/¹³C ratio is a good tracer of the stellar nucleosynthesis and the evolutionary stage.

The advantage of using the isotopic ratios lies in the reliability of the ratios compared to the absolute abundance values, since the ratios are less dependent on the limitations of modelling and observational errors that affect the absolute values.

From an observational point of view, direct measurements of elemental photospheric ratios are very challenging and sometimes impossible with current observational techniques. Hence, observations of circumstellar molecules, which possess permanent dipole moments and are thus observable at radio/mm/sub-mm frequencies, are extensively used as tracers of the elemental photospheric ratios. Observations of the circumstellar ¹²CO/¹³CO are widely used to trace the elemental

photospheric $^{12}\text{C}/^{13}\text{C}$ ratio in the CSEs (e.g. Groenewegen et al. 1996; Greaves & Holland 1997; Schöier & Olofsson 2000; Milam et al. 2009). However, discrepancies between the photospheric $^{12}\text{C}/^{13}\text{C}$ and the circumstellar $^{12}\text{CO}/^{13}\text{CO}$ ratios have been observed for a number of AGB stars. In this work, we study the processes responsible for the discrepancy between the circumstellar molecular isotopologue ratios and the elemental photospheric isotope ratios.

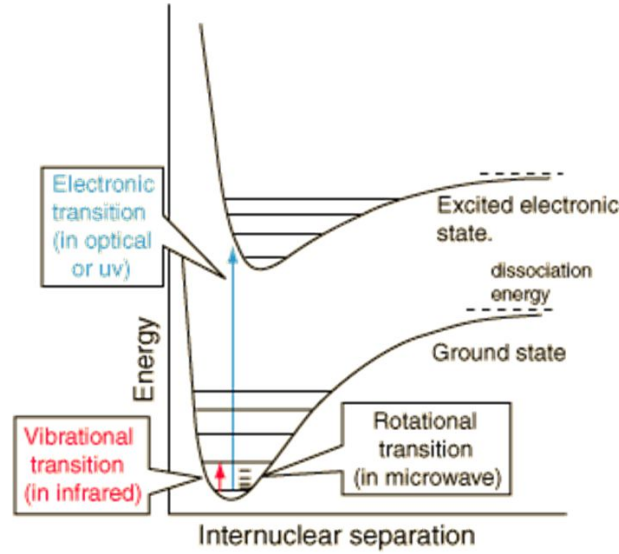
The chemical reactions are not expected to affect the isotopologues abundance ratios. However, the photochemical reactions are able to change the isotopologues ratios of molecules with sharp discrete absorption bands in UV such as isotopologues of H_2 , CO , N_2 , C_2H_2 , NO in UV irradiated regions (e.g. Lee 1984; Savage & Sembach 1996; Visser et al. 2009). Moreover, ion- molecule charge- exchange reactions in low temperature regions (outer CSE) can also change the isotopologue abundance ratios (e.g. Watson et al. 1976). Therefore, a proper treatment of the photodissociation of molecules that are photodissociate through lines are required in deriving the isotopologues ratios of CSEs. A detailed discussion on the molecular photodissociation and potential UV radiation fields that may affect the chemistry of CSEs are discussed in Chapter 3.

Radiative Transfer Modelling

All the information that we have from the stars comes from observations of electromagnetic radiation which forms and transfers through the interaction with baryonic matter. Thus, in order to analyze astronomical spectra, understanding of the interaction between radiation and material is required. The interaction of radiation and matter is governed by different atomic and molecular processes. In this chapter, different molecular transitions responsible for the astronomical spectra, the transfer equation for radiation propagating through matter, and finally the method of solving the radiative transfer equation used in the appended paper will be discussed.

2.1 Molecular transitions

The molecular transitions can be divided into three categories. Figure 2.1 shows the potential energy versus the internuclear distance for different molecular states. The most energetic molecular transitions are electronic transitions which are observable in visual or UV regions of the spectrum. Vibrational transitions occur between different vibrational levels of the same electronic state and are mostly observable in the infrared region of the spectrum. The available vibrational modes, stretching and bending the bonds between atoms of a molecule, strongly depend on the structure of the molecule. The least energetic molecular transitions are rotational transitions which occur between rotational levels of the same vibrational state. Rotational transitions lie at longer wavelengths in millimetre and radio. Polar molecules which possess permanent dipole moments such as CO have rotational transitions. However, homonuclear diatomic molecules like H₂, N₂, which don't have a permanent electronic dipole, can not undergo the allowed rotational transitions. We exclusively observe the rotational transitions of polar molecules in the CSEs of AGB stars in radio/millimeter/submillimeter wavelengths. In order



<http://hyperphysics.phy-astr.gsu.edu/hbase/molecule/molspecon.html#c1>

Figure 2.1: A schematic view of the adiabatic potential curve shows the electrical potential energy versus the internuclear separation.

to model the observational spectra, resulting from different transitions, we need to calculate the populations of all the involved levels and the probability of different transitions, which will be discussed in the following sections.

2.2 Radiative rates

The probabilities or rates of different transitions between two energy levels u and l ($E_u > E_l$) consist of spontaneous emission, stimulated emission and absorption, can be expressed by Einstein coefficients as in the following.

The spontaneous emission rate per unit time (s^{-1}) for a transition from an upper state u to a lower state l with the frequency $\nu_{ul} = (E_u - E_l)/h$ is

$$A_{ul} = \frac{8\pi^2\nu^3}{3\epsilon_0\hbar c^3} |\mu_{ul}|^2, \quad (2.1)$$

where μ_{ul} is the transition dipole moment (this indicates the electric dipole moment associated with the transition between the two states), ϵ_0 is the permittivity of free space, c is the speed of light in a vacuum and $\hbar = h/2\pi$ where h is Planck's constant. This spontaneous transition releases a photon with the energy $h\nu = E_u - E_l$.

The rate of stimulated emission is defined as:

$$B_{ul} = \frac{|\mu_{ul}|^2}{6\epsilon_0\hbar}. \quad (2.2)$$

Two rates of spontaneous and stimulated emission are related via:

$$A_{ul} = \frac{8\pi h\nu^3}{c^3} B_{ul}. \quad (2.3)$$

And finally the rate of stimulated absorption can be written in terms of the stimulated emission rate

$$B_{lu}g_l = B_{ul}g_u, \quad (2.4)$$

where g_l is the statistical weight of level l.

In addition to the interaction of molecules and the electromagnetic radiation, the molecular transition between energy levels can also occur through collision of a molecule with other abundant species such as H₂ and He. In the CSEs of AGBs, H₂ is the most abundant molecule and because of that we consider its collisional rate with the molecule of interest in the modelling. The rates of collision-induced transitions C_{ul} depends on the number density of collision partner n_c and the collisional de-excitation rate q_{ul} in cm³s⁻¹

$$C_{ul} = n_c q_{ul}. \quad (2.5)$$

The upward and downward collisional rate coefficients can be related by

$$q_{lu} = q_{ul} \frac{g_u}{g_l} e^{-(E_u - E_l)/kT_{kin}}, \quad (2.6)$$

where g_u is the statistical weight of the level u. The upward collisional rate q_{lu} are related to the fundamental excitation cross section σ_{lu} by

$$q_{lu} = \left(\frac{8kT_k}{\pi\mu}\right)^{-1/2} (kT_k)^{-2} \int \exp(-\epsilon/kT) \sigma(\epsilon) \epsilon d\epsilon, \quad (2.7)$$

where ϵ is the collision energy and μ is the reduced mass of molecule collider system.

2.3 Radiative Transfer Modelling

The specific intensity of a radiation field is defined as the energy flux per unit time, frequency, solid angle and area normal to the direction of propagation. This energy is constant while the ray passes through vacuum. However, propagation of radiation through matter causes changes in the specific energy due to emission

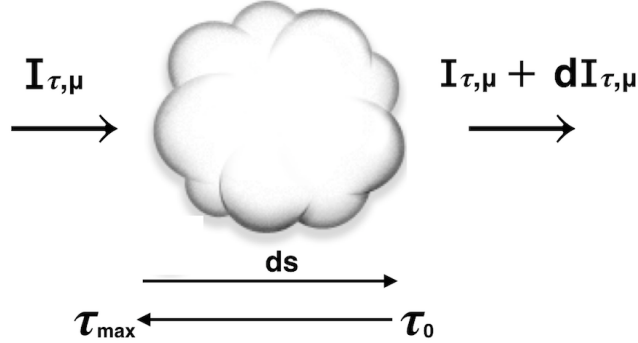


Figure 2.2: Illustration of the propagation of radiation through a cloud with a geometrical depth ds and an optical depth τ .

(spontaneous and stimulated), absorption and scattering (Fig. 2.2). In the absence of scattering, the changes in a beam after passing a distance ds through matter is given by

$$\mu dI_{\mu\nu} = j_{\mu\nu} ds - \kappa_{\mu\nu} I_{\mu\nu} ds, \quad (2.8)$$

where $j_{\mu\nu}$ is the spontaneous emission coefficient, $\kappa_{\mu\nu}$ is the absorption coefficient at frequency ν and $\mu = \cos\Theta$ is the direction cosine of the angle Θ between the propagation direction and the outward normal direction. In this equation, the first term indicates the intensity added to the beam by spontaneous emission and the second term shows the intensity subtracted from it by absorption.

The radiative transfer equation describes how intensity varies with depth through a medium. The transfer equation for radiation corresponding to a transition from u to l at frequency ν propagating a distance ds through a medium can be written as:

$$\mu \frac{dI_{\mu\nu}}{ds} = j_{\mu\nu} - \kappa_{\mu\nu} I_{\mu\nu}. \quad (2.9)$$

The transition probabilities were discussed in section 2.2 can be used to construct the absorption and emission coefficient in great detail over a broad range of photon energies.

The emission coefficient for a transition between levels u and l can be written as:

$$j_{\mu\nu} = \frac{h\nu_{ul}}{4\pi} n_u A_{ul} \phi(\mu, \nu), \quad (2.10)$$

where n_u is the number density in level u , and $\phi(\mu, \nu)$ is the normalised Doppler profile for the emission line which describes the relative effectiveness of frequencies near ν for causing transitions.

The absorption coefficient for a spectrum line is given by:

$$\kappa_{\mu\nu} = \frac{h\nu_{ul}}{4\pi} \phi(\mu, \nu) (n_l B_{lu} - n_u B_{ul}). \quad (2.11)$$

The absorption coefficient integrated over path-length through the atmosphere gives a quantity, optical depth, which describes the opacity of the material in it. Indeed, the optical depth counts the number of photon mean free paths along the direction ds and can be defined

$$d\tau = \int \kappa_{\mu\nu} ds. \quad (2.12)$$

If we replace the geometrical depth ds with an optical depth $d\tau$ defined above, the radiative transfer equation 2.9 can be written

$$\frac{dI_{\mu\nu}}{d\tau} = S_{\mu\nu} - I_{\mu\nu}, \quad (2.13)$$

where $S_{\mu\nu} = j_{\mu\nu}/\kappa_{\mu\nu}$ is called the source function at the transition frequency. The source function for a transition between states u and l can be expressed by the Einstein coefficients as

$$S_{ul} = \frac{n_u A_{ul}}{n_l B_{lu} - n_u B_{ul}}. \quad (2.14)$$

The solution for the simplified transfer equation 2.13 can be written

$$I_{\mu\nu} = I_{\mu\nu}(0) \exp(-\tau) + \int_0^\tau S_\nu(\tau') \exp(-(\tau - \tau')) d\tau', \quad (2.15)$$

the first term represents the amount of radiation absorbed from the background intensity $I_{\mu\nu}(0)$ and the second term accounts for the radiation emitted and re-absorbed within the atmosphere.

In order to solve the radiative transfer equation, the molecular level populations are required. In calculating the molecular level populations, we consider that there is a balance between all the upward and downward processes which populate and de-populate each state i of a molecule, which is called the statistical equilibrium (SE). In the SE condition, all the rate equations can be written:

$$\frac{dn_i}{dt} = 0, \quad (2.16)$$

thus, the statistical equilibrium system of equations can be written:

$$\sum_{l < u} [n_u A_{ul} - (n_l B_{lu} - n_u B_{ul}) \bar{J}_{ul}] - \sum_{l > u} [n_l A_{lu} - (n_u B_{ul} - n_l B_{lu}) \bar{J}_{ul}] + \sum_{u, l} (n_u C_{ul} - n_l C_{lu}) = 0, \quad (2.17)$$

where \bar{J} is the mean intensity obtained by integrating the specific intensity over solid angle Ω and averaged over all directions μ and can be written as:

$$\bar{J} = \frac{1}{4\pi} \int d\Omega \int d\nu \varphi_{ul}(\mu\nu) I_{\mu\nu}, \quad (2.18)$$

where $I_{\mu\nu}$ is the specific intensity along direction μ with frequency ν and $\varphi(\mu\nu)$ is a weight function.

2.4 Accelerated Lambda Iteration method

One of the commonly used direct methods of solving the radiative transfer equation is the Accelerated Lambda Iteration (ALI) method. The ALI method is described in detail by (e.g. Scharmer 1981; Rybicki & Hummer 1991). The code, which is used in the first paper, is based on the ALI method and has been implemented by Per Bergman. It was used in modelling of the CSE of AGB stars by (e.g. Maercker et al. (2008, 2009); Danilovich et al. (2014) and Saberi et al. (2016)).

In the ALI method, $I_{\mu\nu}$ will be derived by using an operator Λ which is acting on the source function S and gives the specific intensity at any radial point as the following

$$I_{\mu\nu} = \Lambda_{\mu\nu}[S_{tot}(\mu\nu)] + L_{bg}, \quad (2.19)$$

where the source function S_{tot} includes all contribution from dust and overlapping lines and L_{bg} is contribution from the background. The Λ operator is a $N \times N$ dimensional matrix where N is the number of radial points. The diagonal elements describe the local contribution and the off-diagonal elements count the contribution from other parts of the cloud.

The code starts with an initial guess for the level populations to solve the statistical equilibrium (SE) equation (Eq. 2.17). Then, the specific intensity will be calculated at any radial points (Eq. 2.18). The derived populations from the last iteration will be used to solve a new SE equation. This process is continued until convergence in the level populations is obtained.

The effect of UV radiation on the chemistry in CSEs

3.1 Potential UV-radiation fields

Circumstellar envelopes (CSEs) are photon dominated regions. Thus, UV-radiation impacts the chemistry of the CSEs around evolved stars. The potential UV sources that can penetrate through CSEs are the interstellar radiation field (ISRF) from outside and stellar chromospheric activity from inside. In binary systems, active binary companions can emit UV-radiation from the inner side as well. A more detailed discussion on the UV-radiation sources are presented in the following subsections.

Photodissociation of the molecular gas is thought to be dominated by the interstellar UV-radiation while the star is in the AGB. However, a recent search for UV emission from AGB stars has revealed that 180 AGB stars, $\sim 50\%$ of which were observed with Galaxy Evolution Explorer (GALEX), have detectable near- or far-UV emission (Montez et al., in prep). This supports the possible existence of an internal source of UV-radiation. There is little research on the influence of internal UV sources on the physical and chemical conditions of CSEs, since previous studies are mostly based on low-resolution single-dish observations which are unable to resolve such effects. In this work, we aim to pay particular attention to the effect of UV radiation either from a binary companion or the chromospheric activity on the chemistry of the CSEs.

3.1.1 External UV radiation - ISRF

The ISRF is the only UV radiation field which has been considered to influence the chemistry of CSEs in many studies. However, a more precise treatment of the ISRF penetration through the CSE is still needed. The penetration of the ISRF depends

on several parameters such as the strength of the local ISRF, the CSE geometry and the degree of clumpiness, the dust composition and anisotropy of the scattered radiation. Observations have shown that CSEs have clumpy structures both on small and large scales (e.g. Chapman et al. 1994; Guélin et al. 1997; Weigelt et al. 1998; Fong et al. 2003; Leão et al. 2006). A clumpy circumstellar medium allows the interstellar UV-radiation to penetrate deeper into the envelope compared to a uniform envelope with the same average column density (Meixner et al. 1992) and have significant impact on the chemical composition (e.g. Lee 1984; Agúndez et al. 2010). The degree of clumpiness (or volume filling factor) in the winds of AGBs is not well characterised. Another factor influencing the intensity of the ISRF is the spatial position of the source. Since the main ISRF UV sources, which are hot O and B type stars, are not symmetrically distributed in the galaxy, the ISRF source function depends on the spatial position of the source in the galaxy (Murthy & Henry 1995).

In addition, Goicoechea & Le Bourlot (2007) show that the FUV penetration depends on the dust albedo and anisotropy of the scattered radiation. Consequently, the grain properties and growth must be taken into account. These are different from source to source. The assumption of uniform dust properties and average extinction curves can be a crude approximation to determine the resulting scattering properties. This might affect the modelling results of molecules which are mostly radiatively excited.

3.1.2 Internal UV radiation - Chromospheric activity

The chromosphere is a layer of plasma overlying the photosphere where the temperature goes from ~ 4000 to 25000 K and the density drops quickly. In the stellar photosphere in radiative equilibrium (RE) condition, energy transport through the plasma is purely by radiation. Unlike the photosphere, the chromosphere is not in RE. Thus, non-thermal mechanism of energy deposition must be present. Magnetic and acoustic heating are potential sources for heating the stellar chromospheres.

Previous studies of UV-spectra indicate the presence of a chromosphere in the outer atmosphere of giant stars (e.g. Hartmann et al. 1982; Querci & Querci 1985; Johnson et al. 1986; Eaton & Johnson 1988; Judge & Stencel 1991; Schrijver 1995; Carpenter et al. 1997). Observations of several emission features of high temperature ionized species such as Fe(II), Ca(II), C(II) from cool stars are the observationally tracers of the stellar chromospheres. Moreover, emission lines such as Ca(II), H and K are a sure sign of departure from RE condition, and thus the chromospheric origin emission. However the chromospheric UV emission has been ignored in the recent modelling of the CSEs due to its complexity.

3.1.3 Internal UV radiation - Binary companions

Binarity has been offered as a possibility to explain the shape of planetary nebulae (PNe) or asymmetries in the CSE of AGBs. However, the rate of binarity in evolved stars is not precisely known. The discovery of hot companions is more straightforward when the companion is hot such as a white dwarf, but the detection of low- to intermediate MS companions is not straightforward. Sahai et al. (2008) and Ortiz & Guerrero (2016) report the detection of UV-radiation for a sample of AGBs, interpreted as arising from a hot embedded companion. Although, it should be noted that, they have not even considered the possibility of the UV radiation by the AGB star.

In this work, to study the effect of the internal UV radiation either by the chromospheric activity or binary companions in the C-type AGB stars, we suggest observations of the isotopologue ratios of the most abundant C-bearing species in the CSEs. This is an indirect way of measuring the effect of UV radiation on the chemical composition of CSEs. In the case of binary systems, it may be an direct way of detecting binary companions which are challenging or impossible to directly observe by the current observing tools. However, distinguishing between the two internal UV radiation (binary and stellar activity) requires high spatial resolution observations of the photodissociated products of parent species. Morphology of the molecular gas of photodissociated species may reveal the origin of UV radiation field. Moreover, UV Spectroscopic observations by Hubble space telescope (HST) can provide valuable information to quantify the internal UV radiation.

3.2 Molecular photodissociation by UV radiation

Molecular photodissociation by UV radiation can dominate by direct photodissociation or indirect photodissociation mechanisms, Fig 3.1. In the direct photodissociation process, a molecule absorbs the photon into a repulsive excited electronic state. Thus, the photodissociation cross section is continuous as a function of photon energy. In this case, all the absorptions lead to the molecular dissociation, since spontaneous emission back to the ground state is comparatively slow (typical Einstein-A coefficients of 10^9 s^{-1} compared with dissociation times of 10^{13} s^{-1}). The photodissociation rate in s^{-1} by continuous absorption can be expressed by

$$k_{pd}^{cont} = \int \sigma(\lambda) I(\lambda) d(\lambda), \quad (3.1)$$

where σ is the photodissociation cross section in $[\text{cm}^2]$ and I is the mean intensity of the radiation in $[\text{photons cm}^{-2} \text{ s}^{-1} \text{ \AA}^{-1}]$ as a function of wavelength λ in $[\text{\AA}]$.

The indirect photodissociation is a two step process. A molecule absorbs the

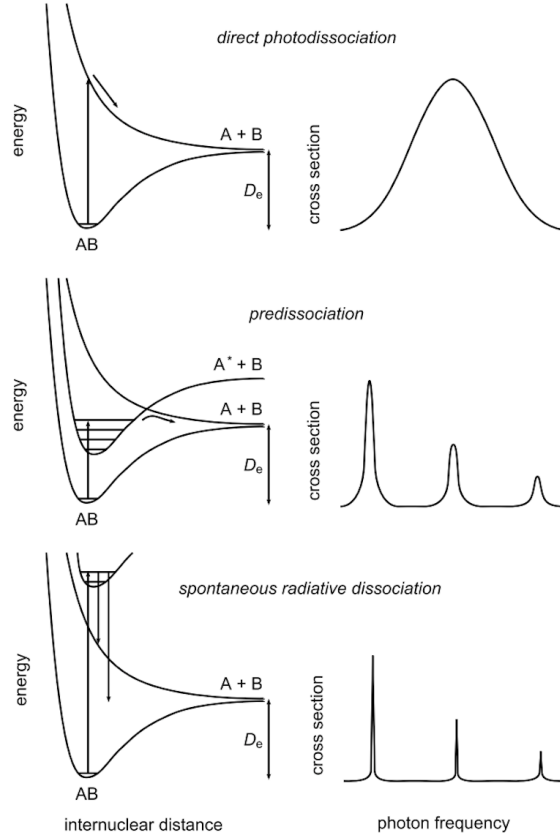


Figure 3.1: Photodissociation processes of diatomic molecules and corresponding cross sections. From top to bottom: direct photodissociation, predissociation and spontaneous radiative dissociation from van Dishoeck & Visser 2015 (arXiv:1106.3917).

photon to a bound electronic state and the bound electronic state interacts non-radiatively with a nearby repulsive electronic state. The photodissociation cross section contains a series of discrete peaks. In this case, the photodissociation rates are comparable with the spontaneous emission rates. In the case that the excited bound states are not predissociated, spontaneous radiative dissociation can occur by emission of photons into the continuum of a lower repulsive state or the vibrational continuum of the ground electronic state. The photodissociation cross section again contains a series of discrete peaks. A more detailed discussion can be found in van Dishoeck & Visser (2015). The photodissociation rate between levels u and l by an indirect process is given by

$$k_{pd}^{line} = \frac{\pi e^2}{mc^2} \lambda_{ul}^2 f_{ul} \eta_u x_l I(\lambda_{ul}), \quad (3.2)$$

where f_{ul} is the oscillator strength which express the transition probability, η_u is the

dissociation efficiency of the upper level and x_l indicates the fractional populations of the level l .

In principle all of the above processes will occur, since a molecule has many excited electronic states that can be populated by the ambient radiation field.

The main factor determining domination of line or continuous dissociation process is the structure of the molecule. For instance, photodissociation processes of e.g. H_2 , CO , N_2 , which are also the most abundant molecules in astrophysical regions, are dominated by line dissociation, while HCN is photodissociated via continuum.

The photodissociation rate of molecules with sharp absorption bands in the UV, depends on the molecular column densities. Because all the relevant photons that can dissociate the molecules in deeper regions of the cloud have been already absorbed by the molecules near the exposed region. Thus, the molecules in the deeper regions are shielded from dissociation which is called molecular self-shielding. As a consequence, two isotopologues of a molecule with different column densities are not equally affected by the same UV radiation. This causes the changes in the isotopologue ratios in UV irradiated regions. While, isotopologues of molecules with continuum dissociation are equally affected by the radiation field. Consequently, comparison between the isotopologue ratios of molecules which are dissociated by line (e.g. CO) and continuum (e.g. HCN) will help to quantify the effect of UV radiation. We will use this to study the effect of internal UV radiation in the CSEs of AGBs.

Chemical Modelling

To do the chemical modelling of the CSEs around AGB stars, we are using a modified version of the publicly available code, *rate13-cse-code*¹, hereafter CSE code. A brief description of the code and the applied modifications are presented in the following section. A more detailed discussion on the code can be found in the paper by McElroy et al. (2013).

4.1 The CSE code

The code assumes that a CSE is a spherically symmetric envelope which is formed due to a constant mass loss from an evolved star. The envelope is expanding with a constant velocity v_e . The mass loss rate \dot{M} and the expansion velocity v_e are two free parameters which determine the H₂ number density distribution throughout the envelope $n_{H_2}(r)$, which falls as $1/r^2$ (r is the distance from the central star). The temperature distribution profile is assumed to be a power-law

$$T(r) = T_i \left(\frac{r}{r_i}\right)^{-n}, \quad (4.1)$$

where n is typically assumed to be $n = 0.6 - 0.7$, and T_i is the temperature at the inner radius r_i .

The user can set the initial abundance of parent or photospheric species relative to H₂. The abundances of different circumstellar species relative to H₂ number density, $f_i = n_i/n_{H_2}$, are calculated at each radial point by solving an ordinary differential equation:

$$\frac{df_i}{dr} = \frac{1}{v_e} \left[\sum_{j,k} k_{jk} f_j f_k n(r) + \sum_l k_{li} f_l - f_i \left[\sum_m k_{im} f_m n(r) + \sum_n k_n \right] \right] \text{cm}^{-1} \quad (4.2)$$

¹<http://udfa.ajmarkwick.net>

Table 4.1: reactions type which are considered in the chemical network of the CSE code.

Code	Reaction type	Reaction rate
AD	Associative Detachment	$k_1 = \alpha \left(\frac{T}{300}\right)^\beta \exp\left(\frac{-\gamma}{T}\right) [\text{cm}^3 \text{s}^{-1}]$
CD	Collisional Dissociation	k_1
CE	Charge Exchange	k_1
CP	Cosmic-Ray Proton (CRP)	$k_2 = \alpha [\text{s}^{-1}]$
CR	Cosmic-Ray Photon (CRPHOT)	$k_3 = \alpha \left(\frac{T}{300}\right)^\beta \frac{\gamma}{1-\omega} [\text{s}^{-1}]$
DR	Dissociative Recombination	k_1
IN	Ion-Neutral	k_1
MN	Mutual Neutralisation	k_1
NN	Neutral-Neutral	k_1
PH	Photo Process	$k_4 = \alpha \exp(-\gamma A_v) [\text{s}^{-1}]$
RA	Radiative Association	k_1
REA	Radiative Electron Attachment	k_1
RR	Radiative Recombination	k_1

NOTE: In the reaction rates T is the gas temperature. In: k_1 : α is pre-exponential factor, β indicates the temperature dependence of the rate coefficient and γ is the activation energy of the reaction. k_2 : α is the cosmic-ray ionisation rate. k_3 : α is the cosmic-ray ionisation rate, γ is the probability per cosmic-ray ionisation that the photo-reaction takes place and ω is the dust-grain albedo. k_4 : α is the photodissociation rate in the unshielded region, A_v is the extinction by the interstellar dust at visible and γ is a parameter to take into account the increased extinction at ultra-violet wavelengths compared to the visible.

where the two first terms count all the reactions which lead to creation of the species i by two-body reactions and photo-processes respectively. The two last terms count all the reactions which lead to destruction of the species i . The rate coefficient for each reaction is given by k . Table 4.1 presents all the reaction types and rates which are considered in the chemical network of the code.

4.1.1 The chemical network

We have upgraded the chemical network of the CSE code to contain ^{13}C and ^{18}O isotopes and their bearing species. Chemical fractionation reactions have been added to the chemical network as well. The number of species and chemical reactions of the publicly available version and the updated version are given table 4.2. Figure 4.1 shows our first preliminary results from the updated version of the code which contains the ^{13}C and ^{18}O isotopes. In this model the mass loss rate and expansion velocity are assumed to be $\dot{M} = 1.5 \times 10^{-5} M_\odot \text{yr}^{-1}$ and $v_e = 14.5 \text{ km s}^{-1}$ which are the reported values for the C-type AGB star, IRC+10216.

Table 4.2: The number of species and chemical reactions in the CSE code.

The number of	Old version	updated version
Species	466	932
Reactions	6173	15108

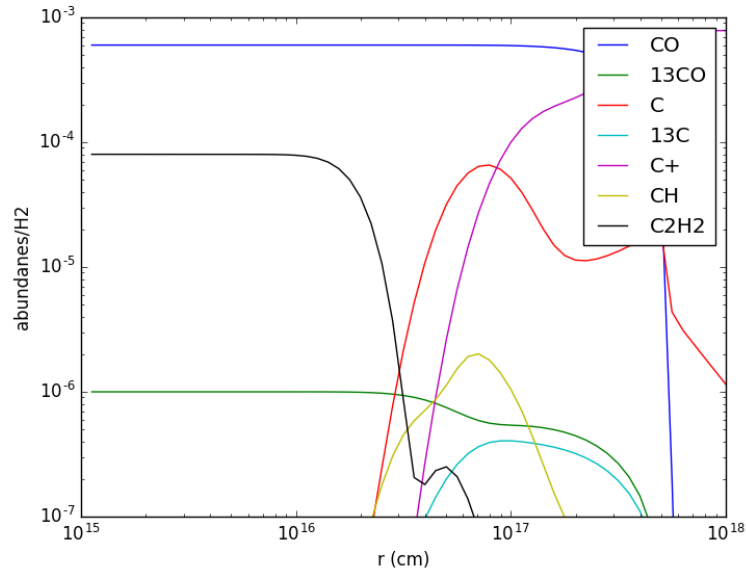


Figure 4.1: The preliminary results from the chemical modelling of a CSE by adding the isotopic chemistry to the CSE code.

4.1.2 Photodissociation of CO

The standard interstellar radiation field derived by Drain et al. 1978 is assumed to irradiate the outer envelope from all directions. The code assumes that CO photodissociates by absorbing photons in one band at 1000 \AA . The CO self-shielding is calculated using a single-band approximation (Morris & Jora 1983). However, generally in the CSEs, self-shielding decreases the line contribution and the dust shielding decreases both line and continuum contributions.

In the CSE code, it is assumed that the photodissociation of CO is entirely by line and is expressed by:

$$k = \sum_i k_{0i} \beta_i, \quad (4.3)$$

where the summation is over each contributing discrete line i (here, one band

at 1000 Å), k_0 is the unshielded photodissociation rate and is assumed to be $k_0 = 2 \times 10^{-10} \text{ s}^{-1}$ at the dissociating frequency. The β shows the penetration probability for a photon within the dissociating molecular line and is approximated by Morris & Jura 1983 to be:

$$\beta_i = \frac{1 - e^{-1.5\tau_i}}{1.5\tau_i} \times \gamma, \quad (4.4)$$

where γ is the attenuation or continuum shielding factor by dust. This can be numerically approximated using:

$$\gamma = \exp(-1.644\tau_d^{-0.86}), \quad (4.5)$$

where τ_d is the dust optical depth at 1000 Å. This is assumed to be:

$$\tau_d = 4.97 \times 10^{-21} \times n_{H_2}. \quad (4.6)$$

In the Eq. 4.4 τ is the effective optical depth of CO which is calculated using:

$$\tau_i = 0.0265 \times f_i \times \chi_i \times \lambda \times n_{H_2} \times X_{CO} \times \frac{1}{v}, \quad (4.7)$$

where f is the fractional population of the lower level. In the low temperature of the CSEs, it can be assumed that only the lowest three rotational levels typically have significant population, thus the fractional population can be set to $f = 1/3$. Here, χ is the oscillator strength and is assumed to be $\chi = 0.017$ at the dissociating frequency.

Implementation of the CO photodissociation by considering all the effective CO dissociating bands as well as considering the $H_2 + H$ shielding from Visser et al. (2009) is under way. After applying these corrections, we aim to add the internal UV radiation and study its effect on the molecular distribution and the isotopologue ratios in the CSEs.

Introduction to Paper I

To study the effect of internal UV radiation on the chemistry in CSEs, we have started the analysis of the carbon-type AGB star, R Scl. Previous studies have shown that the chemical composition in the inner CSE of R Scl is likely influenced by the internal UV radiation.

R Scl is a semi-regular variable with a pulsation period of 370 days at the distance of around 370 pc. A detached shell of gas and dust was created in a high mass-loss rate during a recent thermal pulse around the central star (e.g. González Delgado et al. 2001, 2003; Olofsson et al. 2010; Maercker et al. 2012, 2014). The ^{12}CO emission maps reveal a spiral structure in the outflow, shaped by a previously undetected binary companion. Spatially resolved ALMA observations of ^{12}CO and ^{13}CO in the outflow of R Scl show big differences in the $^{12}\text{CO}/^{13}\text{CO}$ ratio between different parts of the CSE associated with different mass-loss epochs. Vlemmings et al. (2013) find an average value of $^{12}\text{CO}/^{13}\text{CO} \sim 19$ in the detached shell, consistent with the atomic carbon photospheric ratio $^{12}\text{C}/^{13}\text{C} \sim 19 \pm 6$ by Lambert et al. (1986), whereas they derive a lower limit of $^{12}\text{CO}/^{13}\text{CO} > 60$ for the present-day mass loss, shown in Fig. 5.1. Vlemmings et al. (2013) have suggested that the lack of ^{13}CO in the recent mass loss might be due to the extra photodissociation of ^{13}CO by internal UV radiation from the binary companion or chromospheric activity, while the more abundant ^{12}CO would be self-shielded.

In this paper, we have done a detailed radiative transfer modelling of H^{12}CN and H^{13}CN isotopologues. The results are shown in Fig. 5.2. Our analysis shows that the $\text{H}^{12}\text{CN}/\text{H}^{13}\text{CN} = 26.3 \pm 11.9$ ratio is consistent with the photospheric $^{12}\text{C}/^{13}\text{C} = 19 \pm 6$ ratio. This implies that the CO isotopologue selective photodissociation by the internal UV-radiation could be the main reason of the observed discrepancy between CO isotopologue and C isotope ratios in R Scl, as offered by Vlemmings et al. (2013).

In order to distinguish between potential internal UV fields, from the binary companion and chromospheric activity, we have proposed ALMA observations of

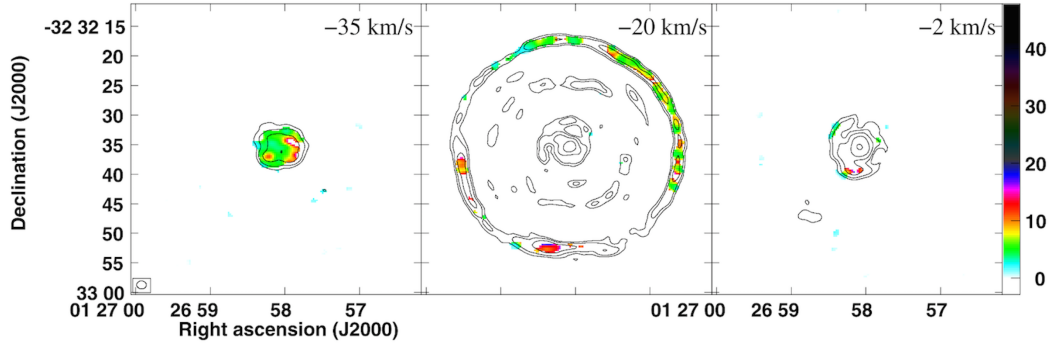


Figure 5.1: Intensity ratio, I_{12CO}/I_{13CO} , (color) and $^{12}CO(J=3-2)$ flux (contours) for three different velocity channels. The ratio is presented where ^{13}CO emission is detected at higher than three σ (where $\sigma = 15 \text{ mJy beam}^{-1}$) and the color scale runs from 0 to 42. The beam size is indicated in the left panel, from Vlemmings et al. 2013.

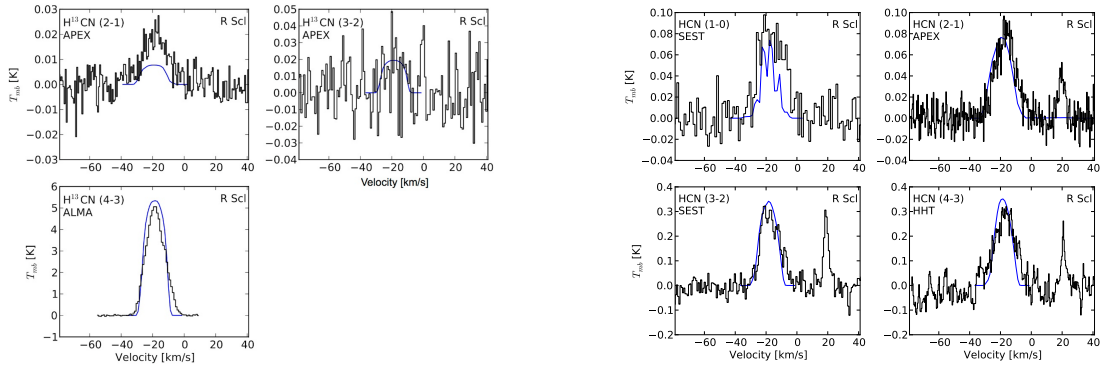


Figure 5.2: $H^{13}CN$ (left panel) and $H^{12}CN$ (right panel) line emissions toward R Scl (Black) overlaid with the model results (Blue). Molecular transitions and the telescopes used to get the data are written in each panel, from Saberi et al. (A&A (2016)).

atomic carbon around R Scl. High spatial resolution of ALMA observations of atomic C, as the main CO photodissociation product, can discriminate between internal UV fields.

Bibliography

- Agúndez, M., Cernicharo, J., & Guélin, M. 2010, *ApJ*, 724, L133
- Bujarrabal, V., Fuente, A., & Omont, A. 1994, *A&A*, 285
- Carpenter, K. G., Robinson, R. D., Johnson, H. R., et al. 1997, *ApJ*, 486, 457
- Castro-Carrizo, A., Quintana-Lacaci, G., Neri, R., et al. 2010, *A&A*, 523, A59
- Chapman, J. M., Sivagnanam, P., Cohen, R. J., & Le Squeren, A. M. 1994, *MNRAS*, 268, 475
- Cherchneff, I. 2006, *A&A*, 456, 1001
- Danilovich, T., Bergman, P., Justtanont, K., et al. 2014, *A&A*, 569, A76
- De Beck, E., Decin, L., de Koter, A., et al. 2010, *A&A*, 523, A18
- De Beck, E., Lombaert, R., Agúndez, M., et al. 2012, *A&A*, 539, A108
- Eaton, J. A. & Johnson, H. R. 1988, *ApJ*, 325, 355
- Fong, D., Meixner, M., & Shah, R. Y. 2003, *ApJ*, 582, L39
- Goicoechea, J. R. & Le Boulrot, J. 2007, *A&A*, 467, 1
- González Delgado, D., Olofsson, H., Schwarz, H. E., Eriksson, K., & Gustafsson, B. 2001, *A&A*, 372, 885
- González Delgado, D., Olofsson, H., Schwarz, H. E., et al. 2003, *A&A*, 399, 1021
- Greaves, J. S. & Holland, W. S. 1997, *A&A*, 327, 342
- Groenewegen, M. A. T., Baas, F., de Jong, T., & Loup, C. 1996, *A&A*, 306, 241
- Guélin, M., Lucas, R., & Neri, R. 1997, in *IAU Symposium*, Vol. 170, *IAU Symposium*, ed. W. B. Latter, S. J. E. Radford, P. R. Jewell, J. G. Mangum, & J. Bally, 359–366

- Habing, H. J. & Olofsson, H., eds. 2003, Asymptotic giant branch stars
- Hartmann, L., Dupree, A. K., & Raymond, J. C. 1982, *ApJ*, 252, 214
- Johnson, H. R., Baumert, J. H., Querci, F., & Querci, M. 1986, *ApJ*, 311, 960
- Judge, P. G. & Stencel, R. E. 1991, *ApJ*, 371, 357
- Lambert, D. L., Gustafsson, B., Eriksson, K., & Hinkle, K. H. 1986, *ApJS*, 62, 373
- Leão, I. C., de Laverny, P., Mékarnia, D., de Medeiros, J. R., & Vandame, B. 2006, *A&A*, 455, 187
- Le Bertre, T. 1997, *A&A*, 324, 1059
- LeBlanc, F. 2010, *An Introduction to Stellar Astrophysics* (Wiley)
- Lee, L. C. 1984, *ApJ*, 282, 172
- Maercker, M., Mohamed, S., Vlemmings, W. H. T., et al. 2012, *Nature*, 490, 232
- Maercker, M., Ramstedt, S., Leal-Ferreira, M. L., Olofsson, G., & Floren, H. G. 2014, *A&A*, 570, A101
- Maercker, M., Schöier, F. L., Olofsson, H., et al. 2009, *A&A*, 494, 243
- Maercker, M., Schöier, F. L., Olofsson, H., Bergman, P., & Ramstedt, S. 2008, *A&A*, 479, 779
- McElroy, D., Walsh, C., Markwick, A. J., et al. 2013, *A&A*, 550, A36
- Meixner, M., Haas, M. R., Tielens, A. G. G. M., Erickson, E. F., & Werner, M. 1992, *ApJ*, 390, 499
- Milam, S. N., Wolf, N. J., & Ziurys, L. M. 2009, *ApJ*, 690, 837
- Murthy, J. & Henry, R. C. 1995, *ApJ*, 448, 848
- Neri, R., Kahane, C., Lucas, R., Bujarrabal, V., & Loup, C. 1998, *A&AS*, 130, 1
- Olofsson, H., Maercker, M., Eriksson, K., Gustafsson, B., & Schöier, F. 2010, *A&A*, 515, A27
- Omont, A., Loup, C., Forveille, T., et al. 1993, *A&A*, 267, 515
- Ortiz, R. & Guerrero, M. A. 2016, *MNRAS*, 461, 3036
- Querci, M. & Querci, F. 1985, *A&A*, 147, 121
- Ramstedt, S., Schöier, F. L., Olofsson, H., & Lundgren, A. A. 2008, *A&A*, 487, 645

- Rybicki, G. B. & Hummer, D. G. 1991, *A&A*, 245, 171
- Sahai, R., Findeisen, K., Gil de Paz, A., & Sánchez Contreras, C. 2008, *ApJ*, 689, 1274
- Savage, B. D. & Sembach, K. R. 1996, *ARA&A*, 34, 279
- Scharmer, G. B. 1981, *ApJ*, 249, 720
- Schöier, F. L. & Olofsson, H. 2000, *A&A*, 359, 586
- Schrijver, C. J. 1995, *A&A Rev.*, 6, 181
- Visser, R., van Dishoeck, E. F., & Black, J. H. 2009, *A&A*, 503, 323
- Vlemmings, W. H. T., Maercker, M., Lindqvist, M., et al. 2013, *A&A*, 556, L1
- Watson, W. D., Anicich, V. G., & Huntress, Jr., W. T. 1976, *ApJ*, 205, L165
- Weigelt, G., Balega, Y., Bloeker, T., et al. 1998, *A&A*, 333, L51

